FLUID WAVES IN RENAL TUBULES

TENEI SAKAI, DANIEL A. CRAIG, ANTHONY S. WEXLER, AND DONALD J. MARSH
Department of Physiology and Biophysics, University of Southern California School of Medicine, Los Angeles, California 90033

ABSTRACT   Autoregulation of renal blood flow is ineffective when arterial pressure perturbations occur at frequencies above 0.05 Hz. To determine whether wave propagation velocity to the macula densa is rate limiting, we estimated compliances of the proximal tubule and the loop of Henle, and used these values in a model of pressure and flow as functions of time and distance in the nephron. Compliances were estimated from measurements of pressures and flows in early proximal, late proximal, and early distal tubules in rats under normal and Ringer-loaded conditions. A model of steady pressure and flow in a compliant, reabsorbing tubule was fitted to these results. The transient model was a set of nonlinear, hyperbolic partial differential equations with split, nonlinear boundary conditions, and was solved with finite difference methods. The loop of Henle compliance was larger than the proximal tubule compliance, and impulses in glomerular filtration rate were attenuated in magnitude and delayed in time in the loop of Henle. Simulated step forcings revealed a similar pattern. Periodic variations of GFR were attenuated at frequencies >0.05 Hz, and there was a delay of 5 s between variations in GFR and macula densa flow rate. The high compliance of the loop slows wave propagation to the macula densa and reduces the amplitude of high frequency waves originating in the glomerulus, but other parts of the signal chain also contribute to the slow response of macula densa feedback.

INTRODUCTION

Autoregulation of renal blood flow is mediated, at least in part, by a sensing mechanism in the macula densa that responds to changes in the composition of tubular fluid usually induced by changes in flow rate. The operation of this mechanism, known as tubuloglomerular feedback (TGF), has been studied extensively in the steady state (14, 15, 18). The amplitude of the feedback response has been well characterized, as has its modification under several sets of experimental circumstances. Changes in arterial pressure, the usual trigger for an autoregulatory response, occur in conscious animals at preferred frequencies (1, 3, 12, 19), and it is therefore of some interest to determine the bandwidth in which TGF is effective, as well as the mechanisms that determine the frequency response. Here we will be concerned with factors that limit the high-frequency response of TGF.

A transient increase in arterial pressure in the rat provokes an autoregulatory response after a delay of several seconds (17, 23). We have suggested that a significant but as yet undetermined fraction of this time is required to propagate the fluid disturbance from the glomerulus along the nephron to the macula densa. This propagation delay is probably a consequence of the physical properties of the tubule. In addition, when arterial pressure is made to vary periodically, autoregulation does not occur at forcing frequencies >0.05 Hz. We suggest that the tubule acts as a low-pass filter because of its high compliance. This filterlike action prevents high frequency changes in fluid flow rate from reaching the macula densa. The goal of this work is to estimate the magnitude of the delay and to compare it to the total delay of autoregulation.

The approach we have taken is to derive a set of nonlinear partial differential equations; one equation describes pressure and the other volume flow in a renal tubule as a function of time and distance. The initial boundary condition on the volume flow equation is GFR and the final boundary condition on both equations is outflow resistance of the nephron segments distal to the macula densa. The parameters of the model are well known except for tubule compliance and the outflow resistance. We have therefore measured steady state tubular hydrostatic pressures and flows in rats to provide a data set from which to calculate the compliances of the proximal tubule and the loop of Henle, and the outflow resistance. We then solved the boundary value problem numerically, using different time-dependent glomerular filtration rate (GFR) patterns to force the system and to estimate the fluid propagation delay between the glomerulus and the macula densa. The results suggest that the compliant tubule walls, especially in the loop of Henle, slow propagation of flow disturbances to the macula densa and attenuate high-frequency response, but that other factors also contribute to the overall frequency response of TGF.

METHODS

Experimental Procedures

Experiments were performed on male Sprague-Dawley rats, weighing 260–350 g, anesthetized by intraperitoneal injection of Inactin (Byk, Konstanz, Federal Republic of Germany), 80 mg/kg body weight. The rats were placed on a temperature-controlled micropuncture table to maintain rectal temperature at 37°C; a heat lamp provided fine control of temperature. A tracheostomy was performed, and a polyethylene catheter was placed in the left femoral vein to replace plasma lost during dissection and to infuse ^{125}I-Na-iothalamate for measurement of single nephron glomerular filtration rate (SNGFR). The renal clearance of iothalamate is the same as that of inulin. Blood was sampled from a catheter in the right carotid artery; this catheter was also used to monitor arterial blood pressure. Additional catheters were placed in the right jugular vein for infusion of 1.2% lissamine green to aid in the identification of nephron segments and in the dome of the urinary bladder to drain it. Blood pressure was recorded continuously with a Statham pressure transducer (model P23dB) and a recorder (Gould Inc., Recording Systems Div., Cleveland, OH). Plasma obtained from retired breeder rats was infused at 10 ml/kg/h for 1 h, and 1.5 ml/kg/h thereafter, to replace losses incurred during surgery. Each animal received a continuous infusion of 26 μC of Na-iothalamate in 0.9% NaCl for 160 min; 45 min were allowed to elapse between the beginning of the infusion and the start of tubular fluid collections.

All the animals were surgically prepared for micropuncture of the left kidney. The abdomen was opened with a left subcostal flank incision, and the renal artery, vein, and the ureter were carefully dissected free of surrounding tissue. The kidney was then placed in a Plexiglass cup, supported with cotton, bathed in mineral oil preheated to 37°C, and illuminated with a fiber optic light guide.

Segments of early and late proximal tubules and of early distal tubules were identified by visual inspection during intravenous injection of a 0.1-ml bolus of lissamine green solution. Hydrostatic pressures were measured with the servonulling method (Instrumentation for Physiology and Medicine, San Diego, CA). Micropipettes for the pressure measurements were 3 μm, outside diameter, and were filled with a solution of 1 M NaCl. Collections of tubular fluid were made by standard micropuncture techniques, using sharpened glass micropipettes filled with stained mineral oil. No nephron was used for more than one pressure measurement or flow collection. Collections lasted 3 min and were made at a rate adjusted to maintain a column of mineral oil at a constant position downstream from the collection site. Collections were made from late proximal and early distal tubules for determination of volume flow rate of tubular fluid; SNGFR was measured from these samples and also by collecting from random sites in the proximal convoluted tubule. Radioactivity was measured in a gamma counter (Tracor, Inc., Instrumental Group, Austin, TX). The volume of collected tubular fluid was measured in constant bore capillary glass. SNGFR was calculated by standard methods (16).

Two series of animals were studied. One group was treated as described above and was designated as control; the second group received an additional infusion of 0.9% NaCl intravenously at a rate equal to 10% of the body weight per hour. Collections and measurements in these volume expanded rats were begun at least 90 min after saline infusion was started.

Model

The equations describing the variation of pressure and flow in a compliant, reabsorbing tube at low Reynolds number are

$$\frac{\partial P}{\partial Z} = -\frac{\rho}{\pi R^2}\frac{\partial Q}{\partial t} - \frac{8\eta}{\pi R^4}Q \qquad (1)$$

$$\frac{\partial Q}{\partial Z} = -2\pi R\frac{\partial R}{\partial P}\frac{\partial P}{\partial t} - \Phi(Z), \qquad (2)$$

where t is time in seconds, Z is distance along the nephron in centimeters, P is tubular pressure in dyn · cm^{-2}, Q is flow in cm^{3}s^{-1}, ρ is the density of tubular fluid in gm · cm^{-3}, η is tubular fluid viscosity in poise, R is tubular radius in centimeters, and Φ is the rate of fluid reabsorption cm^2 · s^{-1}.

The derivation of the model equations, given by Young and Marsh (23), was based on local conservation of mass and momentum in an incompressible fluid. The starting point was the usual set of Navier-Stokes equations and the equation of continuity, in cylindrical coordinates (2). Terms for radial velocity were assumed to be negligibly small, laminar flow was assumed, and the equations were integrated over the cross-section area of the tube. The present form of the equations was reached after numerical evaluation of the remaining terms revealed that the convective acceleration terms were 5 orders of magnitude smaller than the others.

Fig. 1 depicts the model. The tubule was divided into three segments, a proximal tubule, a descending limb, and an ascending limb. The lengths of these segments were assumed to be 1.0, 0.3, and 0.3 cm, respectively. The radius in each segment was assumed to be a linear function of the transmural pressure difference. The coefficients of the radius function were further assumed to be constant over the length of each segment. Separate coefficients were evaluated for the proximal tubule and for the loop of Henle, as explained below under "Parameter estimation." Although the morphology of the descending and ascending limbs suggests that the compliances might differ between the two segments, we lacked an independent means for estimating each separately, and we chose therefore to use a single effective compliance for the entire loop of Henle.

The rate of fluid reabsorption in the proximal tubule was approximated as an exponential function of distance, as in

$$\Phi(Z) = C\exp(-DZ), \qquad (3)$$

where Φ is the local rate of fluid reabsorption, and C and D are coefficients to be evaluated from the data. The need for an exponential function in this study arose because the data dictated something other than a constant rate of reabsorption (see below). The values of the coefficients were estimated from measurements made during steady flow conditions, and were then held constant during the simulations of transients. Our formulation derives its justification from the experimental observation that the early proximal tubule reabsorbs fluid most vigorously, and the late portion least vigorously (11). Fluid reabsorption in the descending limb was assumed to be constant with distance, and was calculated as the difference between the flow rate in the late proximal tubule predicted by Eq. 3 and the measured flow rate in the early distal tubule. As with the proximal tubule coefficients, the rate of fluid reabsorption in the descending limb was assumed to remain constant in the transient simulations. Finally, it was assumed that ascending limbs reabsorb no fluid in any of the conditions we simulated.

The boundary conditions of the model were specified as the flow at the beginning of the tubule (SNGFR) and the resistance to fluid flow offered by nephron segments distal to the macula densa. The outflow resistance from the distal tubule decreases as distal tubule pressure increases,
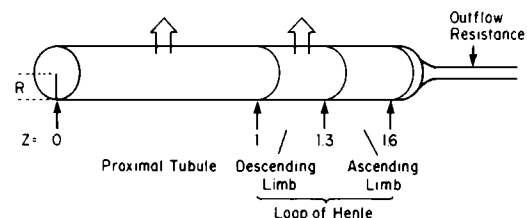

FIGURE 1 The structure of the nephron model. The glomerulus is located at $x = 0$, the descending limb of Henle's loop begins at $x = 1$, the bend of the loop is at $x = 1.3$, and the macula densa is at $x = 1.6$ cm. The early distal tubule begins at a distance of 1.65 cm from the glomerulus.

presumably because the tubule system dilates as local transmural pressure increases (13). Because we wished to simulate experiments in which flow into the distal tubule would vary with time, it was necessary to specify the resistance function and to use it with the instantaneous flow value to calculate pressure. The resistance function was derived from the assumptions that the resistance can be treated as a single, lumped variable, and that the usual laminar flow relationship holds within it. This last assumption implies that the fluid admittance, known from the experimental measurements of pressure and flow in this study, varies with the fourth power of the radius. The fourth-power relationship yields separate values for the effective radius of the lumped admittance in each of the two experimental states we studied. Furthermore, we assumed that the radius was a linear function of the distal tubule pressure, as in Eqs. 4 and 5

$$R_{\omega c} = A_\omega P_c + B_\omega \tag{4}$$

$$R_{\omega ve} = A_\omega P_{ve} + B_\omega, \tag{5}$$

where R_ω is the radius of the outflow resistance, subscripts c and ve refer to control and volume expanded states, respectively, P is the measured pressure in the early distal tubule, and A_ω and B_ω are the parameters to be evaluated. The slope and intercept of the outflow resistance function were evaluated by solving these two equations simultaneously, and the parameter values were used in the calculation of the boundary condition specifying pressure at the end of the simulated tubule.

Numerical Methods

The resulting nonlinear two-point boundary value problem was solved with a finite difference method (20), using centered difference approximations. The time step was 2.5×10^{-2} s. The spatial difference was 0.05 cm, requiring 33 steps for the entire tubule. The zeroth step was the glomerulus, where SNGFR was specified as a boundary condition, and the last step was the macula densa, where the tubular hydrostatic pressure and flow were used to calculate the value of the boundary condition. Halving the spatial step size or the time step did not affect the steady state solution using the transient model.

The local radius was calculated from Eq. 6

$$R_j(Z) = A_j [P(Z) - P_i] + B_j, j = 1, 2 \tag{6}$$

where A_j and B_j are compliance parameters, estimated as described below, the subscript $j = 1$ refers to the proximal tubule and $j = 2$ to the loop of Henle, and P_i is interstitial hydrostatic pressure, assumed to be 5 mmHg (16). $P(Z)$ is the tubular hydrostatic pressure at Z, and was calculated as the average of the pressures at the ith and $(i + 1)$th spatial step in the nth and $(n + 1)$th time step.

The resulting set of finite difference equations formed a bitridiagonal matrix that was solved with an algorithm given by von Rosenberg. The algorithm solved the equations forward in space from the glomerulus to the macula densa, computed the boundary condition at the macula densa with a root-finding scheme, and then solved backward to the beginning of the tubule. This procedure was repeated at each time step until a convergence criterion was satisfied, and then proceeded to the next time step. Convergence was assumed to occur when the Euclidian norm of the solution vector did not change in successive iterations by more than 1×10^{-6}. In all cases, fewer than 10 iterations were required to satisfy the convergence criterion. The finite difference equations are given in the Appendix.

Parameter Estimation

Separate linear approximations of the compliances of the proximal tubule and loop of Henle were assumed, as in Eqs. 7 and 8.

$$R_1(Z) = A_1 P(Z) + B_1 \tag{7}$$

$$R_2(Z) = A_2 P(Z) + B_2. \tag{8}$$

The slope and intercept of these compliance functions were estimated by fitting Eqs. 1 and 2, with the temporal derivatives set to zero, to the values of pressure and flow, measured in experiments under steady flow conditions. The two compliance slopes and two compliance intercepts comprise four unknowns; the differential equations leading to the late proximal and early distal pressures in normal and volume expanded animals comprise the four equations needed to obtain values for these unknowns. The initial conditions for the proximal tubule estimation were the early proximal pressure in the control and volume expansion cases for the pressure equation, and the measured SNGFR values for the flow equation. The measured early proximal tubule pressures were assigned to a point in the model 0.1 cm from the glomerulus, to account for the fact that the earliest accessible measurement site on the surface is downstream from the glomerulus. The measured late proximal pressures and flows were assigned to a point in the model 0.6 cm from the glomerulus, the location of the last accessible measurement site. The rate of tubular reabsorption in the proximal tubule was expressed as an exponential function of distance, as described above.

The initial conditions for the loop of Henle estimations were the pressures and flows at a point 1.0 cm from the glomerulus, and were taken from the solutions of the proximal tubule estimations. The rate of reabsorption in the descending limb of Henle's loop was expressed as a linear function of distance. The initial volume flow rate in the descending limb was taken as the volume flow rate out of the proximal tubule, and the final volume flow was taken to be equal to the early distal volume flow rate, on the assumption that the rate of fluid reabsorption in the ascending limb is zero. The measured early distal tubule pressures and flows were assigned to a point in the model 1.65 cm from the glomerulus.

The flow and pressure equations were integrated forward with a Runge-Kutta fourth-order integration method. The slope and intercept of the linear compliance functions were adjusted iteratively until the com-

TABLE I
SUMMARY OF PRESSURES AND FLOWS

	Tubule site	n	Hydrostatic pressure	Flow rate
			mmHg	*nl/min*
Control	Early proximal	9	13.3 ± .3(18)	31.2 ± 1.1(14)
	Late proximal	9	11.5 ± .3(18)	15.6 ± 1.4(15)
	Early distal	9	7.8 ± .4(13)	9.6 ± 1.0(13)
Volume expansion	Early proximal	7	17.7 ± .4(13)	47.3 ± 3.8(18)
	Late proximal	8	15.1 ± .5(15)	31.7 ± 2.8(10)
	Early distal	7	13.2 ± .3(17)	22.5 ± 3.0(10)

Early proximal flow rate corresponds to SNGFR measured with Na-iothalamate collections. The numbers of individual measurements are in parentheses; n is the number of animals. Averages and SE's were calculated from intraanimal average values.

puted late proximal and early distal pressures matched experimental values in the two experimental states to within 0.01%. These values were obtained with a Newton-Raphson nonlinear equation solving routine. The Newton-Raphson method requires a Jacobian that was calculated with a finite difference method (6).

RESULTS

Experimental Results

The results of flow and pressure measurements made under steady flow conditions are presented in Table I. The flow values under control conditions agree well with reports of similar measurements from several laboratories, especially when care was taken to replace fluid losses from surgery (4, 5, 10, 16). From the standpoint of this study, it is worth noting that the rate of fluid reabsorption in the accessible portion of the proximal convoluted tubule, usually assumed to comprise 60% of its total length, is ~50% of SNGFR. This finding agrees well with the other reports cited, but it implies that the rate of reabsorption in the model cannot be represented as constant over the length of the proximal tubule or else flow rates would be predicted for the distal tubule that are much lower than those measured. Therefore, we have used an exponential approximation of the reabsorption function in the proximal tubule. This formulation is consistent with the set of experimental observations, derived mainly from isolated tubule microperfusion studies, that the S1 segment of the proximal tubule has a higher intrinsic rate of reabsorption than the S2 segment, and that S2 has a higher rate than S3 (11).

The pressure measurements also are in general agreement with those that have been reported for normal rats. The results in Table I reveal a pressure drop along the proximal tubule of 1.8 mmHg. The results of flow measurements in volume-expanded rats are comparable to those we have obtained previously, using the same rate of volume expansion (16). Results of other studies in volume expansion are not directly comparable because different rates of expansion have been used (5, 8). The pressure gradient along the proximal tubule was not significantly different in volume expansion from the gradient found in control animals. The pressure difference between the late proximal tubule and the early distal tubule was significantly less in volume expansion than in controls, despite the fact that volume flow rate more than doubled. Similar observations have been reported earlier (9) and have been explained by comparing the compliance function of the loop of Henle to that of thin-walled rubber tubing.

Compliance Estimates

The data of Table I were used in a steady state version of the model to estimate compliances of the proximal tubule and loop of Henle, under the assumptions that the radius in each segment is a linear function of the local transmural pressure difference, and that the compliance parameters remain constant over the length of each structure. Table II lists the parameters used for this procedure, and Table III the compliance values and the outflow resistance coefficients obtained. The slope of the proximal tubule compliance function was 1.33×10^{-5} cm $\cdot$ mmHg^{-1}, which is in reasonable agreement with the value of 2.25×10^{-5} cm $\cdot$ mmHg^{-1} obtained by Cortell et al., using different experimental methods.

The results indicate that the loop of Henle is a significantly more compliant structure than the proximal tubule. Fig. 2 shows the dependence of tubular pressure in the steady state on these values. As is clear in Fig. 2, the assumption of constant compliance over the length of each segment and the fact that luminal pressure in the loop of Henle is close to the interstitial pressure leads to the prediction that the pressure gradient in the loop of Henle becomes more negative with distance. Thus, the flow resistance appears to be localized to the last fraction of the segment, and is not evenly distributed through the segment. This prediction does not appear to have been tested. An alternative approach might be to assume that the tubular radius and the resistance to flow are constant over the length of each segment, but such a result would require a compliance that varies with distance. There is no justification for assuming a length dependent compliance function, and we have therefore elected to retain the constant compliance assumption.

Fig. 2 also shows the effect on tubular pressure of varying the slope of the compliance function in each segment by 10 or 20%. The effect of varying proximal tubule compliance over this range was minimal. Tubular pressures were more sensitive to variations in the loop of Henle compliance; pressures rose throughout the tubule by 1.1 mmHg when the slope of the compliance function was decreased 20%, and decreased 0.8 mmHg when the slope was increased by 20%. This greater sensitivity of tubule pressure to variation in loop of Henle compliance reflects

TABLE II
PARAMETER VALUES USED IN ESTIMATING TUBULAR COMPLIANCES AND OUTFLOW RESISTANCES

Tubule length		Tubular reabsorption		
	cm		$C, cm^2 \cdot s^{-1}$	D, cm^{-1}
Proximal tubule	1.0	Proximal tubule		
Descending Henle's loop	0.3	Control state	5.6×10^{-7}	1.13
Ascending Henle's loop	0.3	Volume expanded state	5.7×10^{-7}	0.72
		Descending Henle's limb	7.4×10^{-8}	

	Tubule compliance parameters			Distal tubule outflow parameters
	A_j	B_j		
	$cm \cdot mmHg^{-1}$	cm		
Proximal	1.33×10^{-5}	1.31	A_ω	$3.11 \times 10^{-5}\,cm \cdot mmHg^{-1}$
Loop of Henle	2.85×10^{-4}	$-.58$	B_ω	$2.32\,cm$

the interaction of three factors. First, the loop of Henle compliance is greater than the proximal tubule compliance by a factor of ~20; a small percentage change in loop compliance represents a larger absolute change than does the same percentage change in proximal tubule compliance, and the result is a greater effect on tubular radius. Second, the pressure in the lumen of the loop of Henle is nearer to the value of the interstitial pressure than is the pressure in the proximal tubule; small changes in tubule compliance cause a larger change in tubular radius in the loop than in the proximal tubule. Third, this steady state simulation was conducted under the implicit assumption that both GFR and early distal tubule pressure were fixed. Thus, any change in tubular resistance to flow was bound

to have produced an increase in upstream pressure, and the effect would be greater the longer the distance from the glomerulus. These effects, however, are relatively small, and lead to predictions of experimentally reasonable pressures over a 40% range of values. These estimates are therefore likely to be reasonable approximations of the true values, and will be used in the transient simulations that follow.

Simulations of Transients

The general approach used in the following simulations was to use standard, time-dependent forcings on GFR. These included an impulse function, a step, and a sinusoidal forcing pattern. Because the estimates of compliance and outflow resistance were based on linear approximations, we restricted the range of forcings to those that maintained GFR and early distal flow rate to values that were found experimentally and listed in Table I.

Simulated Impulse Functions. We used an impulse-like function to estimate the magnitude of the propagation delay and to identify the tubular segments that attenuate the magnitude of the response. The impulse was given by the following function:
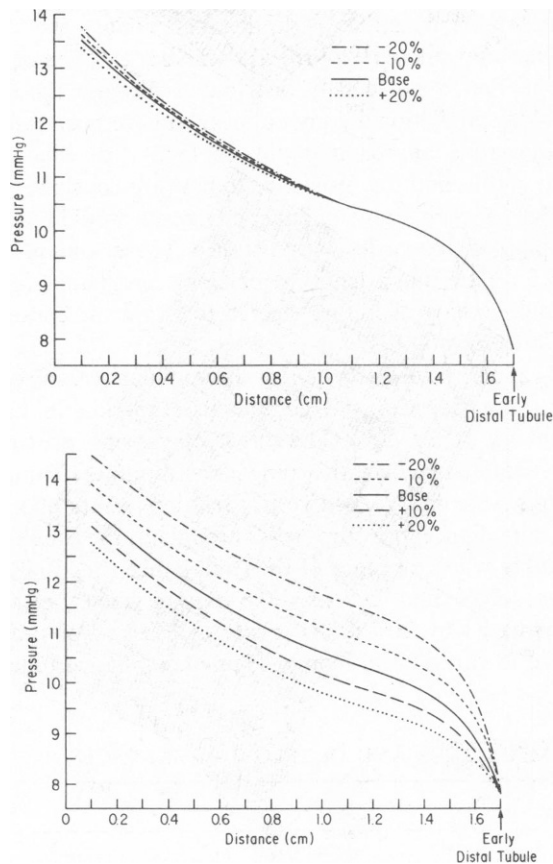
$$GFR(t) = GFR(0) [1 + kEXP(-x^2/2)], \qquad (9)$$

FIGURE 2 The dependence of tubular hydrostatic pressure in normal conditions on the value of the slope of the tubular compliance function. (*Top*) Effect of varying proximal tubule compliance. (*Bottom*) Effect of varying loop of Henle compliance.
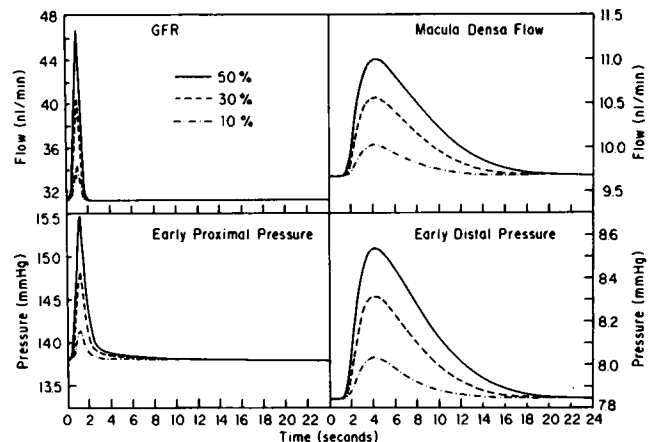
FIGURE 3 The effect on pressure and flow in the early proximal and early distal tubules of imposing an impulse-like change in GFR. Three curves are shown in each panel, representing the response to spikes with maximum amplitude equal to 10, 30, and 50% of the initial GFR. Note the difference in scales between early proximal and early distal responses.

where k is a parameter whose value was selected to provide a curve with a desired maximum value, $x = (t - \tau)/s$, t is the time, τ is the time of occurrence of the maximum value of the function, and s is a parameter that determines its width. In all simulations reported here, the width of the spike was held constant at 0.25 s and the maximum value was varied.

Fig. 3 shows flow and pressure in the early proximal and early distal tubules as functions of time, with maximum impulse heights equal to 110, 130, and 150% of initial GFR. As a test of conservation of mass, the time integral volume flow in the 130% SNGFR impulse was compared with the time integral of the early distal tubule flow response. The two integrals agreed within 0.002, suggesting good conservation of mass.

In all cases, the predicted early distal tubule flow rate lagged several seconds behind the GFR change, was broader, and of smaller amplitude, even though the rate of tubular reabsorption remained constant. The time delay between the peak of the GFR and the peak of the early distal flow change was 3.05 s with the 10% perturbation, 3.15 s with the 30% perturbation, and 3.23 s with the 50% perturbation.

Fig. 4 is a three-dimensional plot of flow and pressure as functions of time and distance, using a spike forcing with a maximum value equal to 150% of initial GFR. Fig. 4 shows some change in the amplitude of the perturbation in the proximal tubule, but most of the broadening and reduction in the amplitude of the flow perturbation occurs in the loop of Henle. The pressure wave caused by the perturbation of GFR was also attenuated primarily in the loop of Henle.

Simulated Step Functions. Fig. 5 shows the results of a simulation with a step increase in GFR of 30% of the initial steady value. The forcing pattern was not a pure step, but an exponential rise with a time constant of ⅙ s. The exponential was chosen to ensure that a stable solution would be obtained. Flow rose more slowly in the early distal tubule than did GFR; the time to reach half the maximum flow at the macuia densa was 10.1 s. Pressure followed flow. Similar patterns were obtained with GFR steps of 110, 120, 140, and 150%, with one additional detail. Fig. 6 shows the time to half maximum flow in the early distal tubule as a function of the magnitude of the increase of GFR. The time to half maximum flow increased with step height. In a strictly linear system, the half-time of response should be independent of the magnitude of the forcing. But tubular pressure increased with the magnitude of the step forcing, tubular radius increased with pressure, and pulse wave velocity varies inversely with the square root of the radius. Thus, we would expect the time to half maximum flow at the macula densa to vary with the magnitude of the step.

Simulated Sinusoidal Functions. Simulations were also performed with sine wave forcings of GFR.

Because the flows and pressures used as an initial condition for these forcings correspond to those measured during the control state in rats, a sine wave forcing necessarily lowers pressures and flows below values that were used to estimate tubular compliances and outflow resistance. We therefore conducted this set of simulations with a variation of GFR that was 1% of the control GFR value.
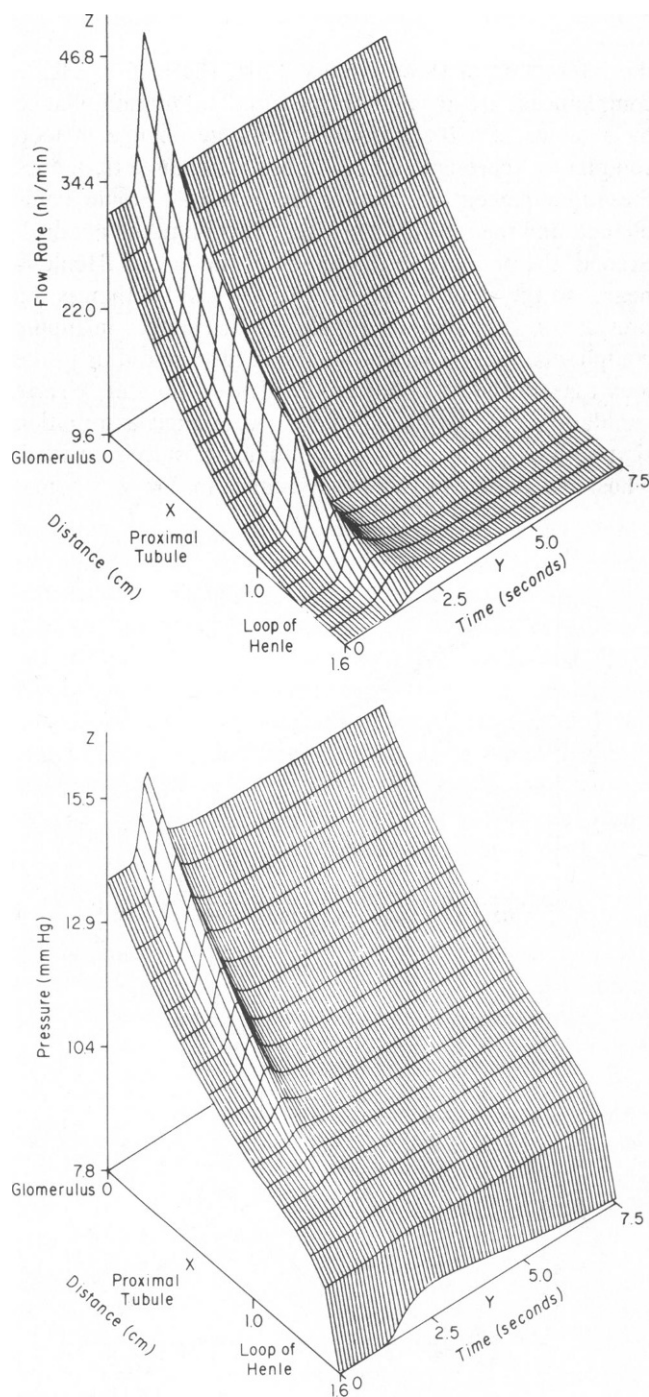

FIGURE 4   Three-dimensional plot showing the variation of pressure and flow as functions of time and distance in a tubule subjected to a spike forcing of GFR with maximum amplitude equal to 50% of the initial GFR.
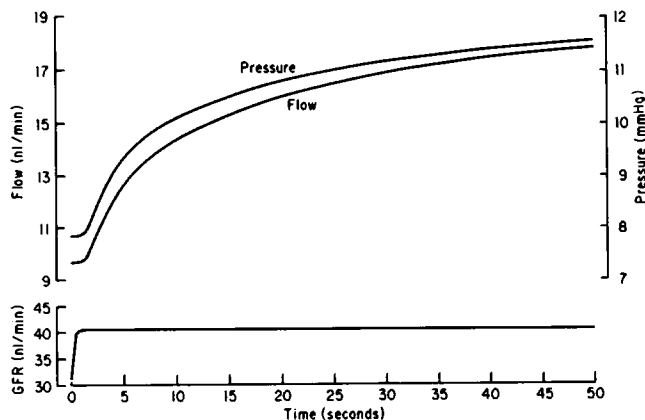
FIGURE 5 The effect on pressure and flow in the early proximal and in the early distal tubule of imposing a steplike change in GFR.

Fig. 7 shows the amplitude of the flow variation at the macula densa as a function of forcing frequency. The flow variation is shown normalized by the amplitude of the GFR variation. Recall that the rate of tubular reabsorption was held constant in all simulations. Thus, the full magnitude of the GFR variation should have appeared in the macula densa flow, unless some dissipative process intervened. The figure shows that the ratio of early distal flow variation to GFR variation was unity only at low frequencies. This ratio declined markedly at higher frequencies. Fig. 7 also displays the time delay between the periodic GFR forcing and the periodic variation in flow at the macula densa. The delay reached a limiting value of 5 s at low frequencies. Experimental studies of autoregulation revealed delays at these frequencies of 20 s (17). These results, when combined with those experimental findings, imply that 15 s of the 20-s delay is attributable to factors other than fluid propagation delays.

DISCUSSION

The motivation for this study was the experimental observation that renal blood flow autoregulation could not respond to perturbations of arterial blood pressure that
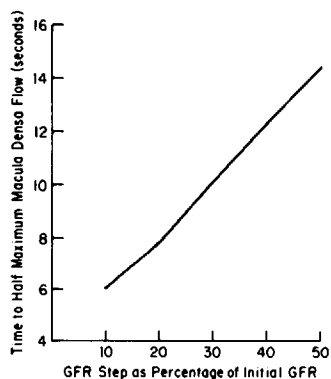

FIGURE 6 Time to half maximum flow in the early distal tubule as a function of the amplitude of the GFR step forcing.
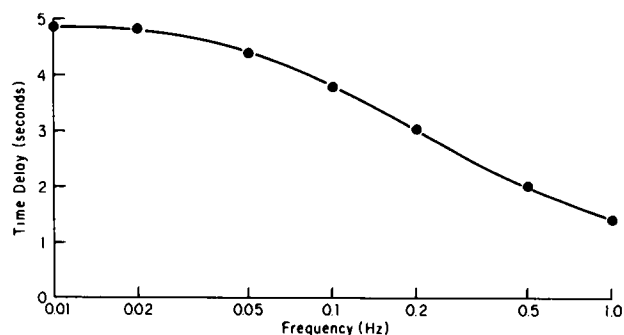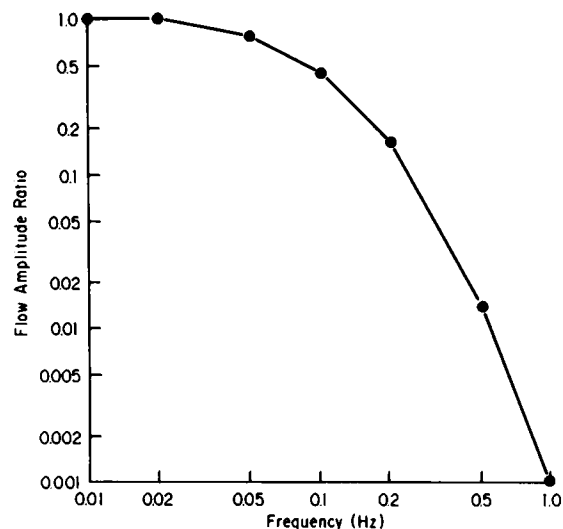

FIGURE 7 Flow variation in early distal tubule during sine wave forcing of GFR, as a function of the forcing frequency. (Top) Amplitude, expressed as a fraction of the amplitude of the GFR forcing. (Bottom) Time delay between zero crossing of GFR and zero crossing of early distal tubule flow.

occurred at frequencies of 0.1 Hz or higher (17). A major signal for renal autoregulation is a change in volumetric flow rate past the macula densa, a collection of specialized epithelial cells at the end of the loop of Henle that communicate with the arterioles that supply blood to the glomerulus of the same nephron. The transport properties of the ascending limb are such that the NaCl concentration in tubular fluid varies monotonically with the flow rate; the resultant change in concentration is the real signal sensed by the macula densa (22). Because the tubules are compliant (7, 9, 21), it is to be expected that the tubular walls can absorb some of the energy of a flow perturbation initiated at the glomerulus. The effect of this high compliance would be that the tubules, and the loop of Henle in particular, serve as a low-pass filter for changes in flow rate, and thus for the autoregulatory responses initiated at the macula densa. The utility of the model lies in its ability to generate estimates of the transfer function and propagation delays of the tubule for comparison with experimental estimates of the same variables measured in the entire blood flow-regulating system.

This boundary-value problem had decided nonlinearities, despite the use of linear approximations for the radius

functions and the boundary condition representing the outflow resistance into the distal tubule. These nonlinearities were unavoidable, because the radius calculation in the tubule and the pressure at the second boundary depended on the reciprocal of the fourth power of the radius. Experimental data suggest that the tubules behave as thin-walled tubing with constant circumference and elliptical cross section at low transmural pressure, but that they are linearly elastic and with circular cross section at higher transmural pressure (9, 21). This behavior can be approximated with a hyperbolic tangent function, among others. We attempted to use such an approximation and were able to obtain stable steady state solutions, but not transient ones. Spike perturbations were not propagated along the proximal tubule, and never reached the macula densa, a prediction that is not consistent with experimental observations (23). Thus, we have been restricted to the use of linear approximations, and we have therefore confined our simulations to circumstances that maintain the calculated dependent variables within the neighborhood of the experimentally determined measurements used to predict the compliances and the outflow resistance.

A major conclusion from this study can be seen in Fig. 4. A simple spike disturbance in GFR was propagated rapidly along the proximal convoluted tubule, and then lost amplitude in the loop of Henle. The high compliance of the loop appeared to delay transmission of the spike, to reduce its magnitude, and to distribute it over a longer period of time; the loop of Henle functioned as low-pass filter. When the disturbance in GFR was periodic, the change in fluid flow rate at the macula densa was attenuated at higher frequencies. The functional implication of this result is that the renal circulation cannot autoregulate at frequencies higher than ~0.05 Hz because the macula densa cannot receive an adequate signal from which to generate an appropriate response.

The time delay between the variations in flow at the glomerulus and at the macula densa, calculated from the periodic forcings, reached a limiting value of 5 s. The rat kidney, tested with periodic variations in arterial pressure, had an average delay of the order of 20 s (17). The calculated delay is consistent with the interpretation that the experimentally observed delay is mediated by the macula densa because the flow change has ample time to reach the sensing site and to initiate a sequence of events leading to adjustments of arteriolar diameter. The results suggest further that other events occupy a significant fraction of the period length at frequencies in the range 0.01–0.05 Hz, and probably to lower frequencies as well. Possibilities include delays in membrane transport in thick ascending limb cells, such that changes in flow rate are not translated immediately into changes in tubular fluid concentrations of NaCl; and time consumed in propagating signals from the macula densa to the arterioles, and converting these signals into an effective action.

Pressure changes in the early distal tubule measured during a step increase in arterial pressure (23) had a time course similar to those shown in Fig. 5. This last comparison supports the validity of the calculated results, and the conclusion that other events in autoregulation consume a significant amount of time. It should also be mentioned that the rat kidneys used for the measurements of frequency response included a population of nephrons longer than those simulated in this study. This other population, the juxtamedullary nephrons comprising ~25% of the total, should have longer propagation times because of their longer length, all other factors being equal. Juxtamedullary nephrons are not available for the measurements that permit the estimation of compliances; computing the time response of a distributed population of nephrons is also a significantly more extensive computational problem than the one we have undertaken here, and we are therefore not able to estimate the magnitude of the effect they might introduce.

In summary, the results of this study are consistent with the hypothesis that the delays inherent in tubuloglomerular feedback operating via the macula densa are responsible for the limited high-frequency response of renal blood flow autoregulation. The tubular compliances, particularly in the loop of Henle, attenuate the propagation of fluid disturbances to the macula densa at frequencies >0.05 Hz, and limit signal access to the feedback pathway. At lower frequencies, changes in GFR are propagated without significant loss, but with time delays that are due in part, but probably not entirely, to the low wave velocities in the tubules. These low velocities are also due to the high tubular compliances.

APPENDIX

The differential equations describing the system are

$$\frac{\partial P}{\partial Z} = - \frac{\rho}{\pi R^2} \frac{\partial Q}{\partial t} - \frac{8\eta}{\pi R^4} Q \qquad (A1)$$

$$\frac{\partial Q}{\partial Z} = - 2\pi R \frac{\partial R}{\partial P} \frac{\partial P}{\partial t} - \Phi(Z). \qquad (A2)$$

Centered difference equations were used for the numerical solution. The approximations are

$$\left(\frac{\partial Q}{\partial Z}\right)_{i-1/2,n+1/2} \simeq \frac{1}{2}\left(\frac{Q_{i,n+1} - Q_{i-1,n+1}}{\Delta Z} + \frac{Q_{i,n} - Q_{i-1,n}}{\Delta Z}\right) \quad (A3)$$

$$\left(\frac{\partial Q}{\partial t}\right)_{i-1/2,n+1/2} \simeq \frac{1}{2}\left(\frac{Q_{i,n+1} - Q_{i,n}}{\Delta t} + \frac{Q_{i-1,n+1} - Q_{i-1,n}}{\Delta t}\right) \quad (A4)$$

$$\left(\frac{\partial P}{\partial Z}\right)_{i+1/2,n+1/2} \simeq \frac{1}{2}\left(\frac{P_{i+1,n+1} - P_{i,n+1}}{\Delta Z} + \frac{P_{i+1,n} - P_{i,n}}{\Delta Z}\right) \quad (A5)$$

$$\left(\frac{\partial P}{\partial t}\right)_{i+1/2,n+1/2} \simeq \frac{1}{2}\left(\frac{P_{i+1,n+1} - P_{i+1,n}}{\Delta t} + \frac{P_{i,n+1} - P_{i,n}}{\Delta t}\right). \quad (A6)$$

Note that the position index, i, has a different value for Q than it has for P. This different indexing was introduced to take into account the fact that

the boundary conditions are split. Q is obtained from

$$Q \simeq \tfrac{1}{4}(Q_{i,n+1} + Q_{i-1,n+1} + Q_{i,n} + Q_{i-1,n}). \qquad \text{(A7)}$$

Setting $dR/dP = A_j$ and substituting Eqs. A3–A7 into Eqs. A1 and A2 yields

$$\frac{\pi R^2}{\rho \Delta Z} (P_{i+1,n+1} - P_{i,n+1})$$

$$+ \left(\frac{1}{\Delta t} + \frac{4\eta}{\rho R^2}\right)(Q_{i,n+1} + Q_{i-1,n+1})$$

$$= -\frac{\pi R^2}{\rho \Delta Z}(P_{i+1,n} - P_{i,n})$$

$$+ \left(\frac{1}{\Delta t} - \frac{4\eta}{\rho R^2}\right)(Q_{i,n} + Q_{i-1,n}) \qquad \text{(A8)}$$

and

$$\frac{1}{2\pi R A_j \Delta Z}(Q_{i,n+1} - Q_{i-1,n+1}) + \frac{1}{\Delta t}(P_{i+1,n+1} + P_{i,n+1})$$

$$= -\frac{1}{2\pi R A_j \Delta Z}(Q_{i,n} - Q_{i-1,n})$$

$$+ \frac{1}{\Delta t}(P_{i+1,n} + P_{i,n}) - \frac{(\Phi_i + \Phi_{i-1})}{2\pi R A_j}. \qquad \text{(A9)}$$

The value of the boundary condition, $Q_{0,n+1}$, was known from the specification of the GFR forcing pattern. An algorithm given by von Rosenberg (20) was used to solve the 64 equations. The algorithm calls for the system to be solved forward beginning at position index $i - 1$ and progressing to $i = 32$. The value of $Q_{32,n+1}$ was then calculated using the value of $P_{33,n}$ and the fourth power relationship between outlet pressure and outlet resistance. A value for $P_{32,n+1}$ was then calculated, and the system of equations was solved backward from position index $i = 32$ to $i = 1$. Convergence was assumed when the Euclidean norm of the solution vector changed $<1 \times 10^{-6}$ in successive iterations.

REFERENCES

1. Akselrod, S., D. Gordon, F. A. Ubel, D. C. Shannon, A. C. Barger, and R. J. Cohen. 1981. Power spectrum analysis of heart rate fluctuation: a quantitative probe of beat-to-beat cardiovascular control. *Science (Wash. DC).* 213:220–222.
2. Bird, R. B., W. E. Stewart, and E. N. Lightfoot. 1960. Transport phenomena. John Wiley & Sons, New York.
3. Blinowska, K., and D. J. Marsh. 1985. Ultra- and circadian fluctuations in arterial pressure and EMG in conscious dogs. *Am. J. Physiol.* 249 *(Regulatory Integrative Comp. Physiol. 18)*:R720–R725.
4. Blantz, R. C., and K. S. Konnen. 1977. Relationship of distal tubule delivery rate and reabsorptive rate to nephron filtration. *Am. J. Physiol.* 233:F315–F324.
5. Brenner, B. M., J. L. Troy, and T. M. Daugherty. 1972. Pressures in cortical structures of the rat kidney. *Am. J. Physiol.* 222:246–251.
6. Carnahan, B., H. A. Luther, and J. O. Wilkes. 1969. Applied Numerical Methods. John Wiley & Sons, New York.
7. Cortell, S., F. J. Gennari, M. Davidman, W. H. Bossert, and W. B. Schwartz. 1973. A definition of proximal and distal tubular compliance. *J. Clin. Invest.* 52:2330–2339.
8. Gottschalk, C. W., and M. Mylle. 1957. Micropuncture study of pressures in proximal and distal tubules and peritubular capillaries of the rat kidney during osmotic diuresis. *Am. J. Physiol.* 189:323–328.
9. Koh, Y. G., and A. D. Baines. 1974. Pressure-flow relationships in Henle's loops and long collapsible rubber tubes. Kidn. Intern. 5:30–38.
10. Kunau, R. T., Jr., H. L. Webb, and S. C. Borman. 1974. Characteristics of sodium reabsorption in loop of Henle and distal tubule. *Am. J. Physiol.* 227(5):1181–1191.
11. Jacobson, H.R. 1979. Characteristics of volume reabsorption in rabbit superficial and juxtamedullary proximal convoluted tubules. *J. Clin. Invest.* 63:410–419.
12. Livnat, A., J. E. Zehr, and T. P. Broten. 1984. Ultradian oscillations in blood pressure and heart rate in free-running dogs. *Am. J. Physiol.* 246:R817–R824.
13. Marsh, D. J., and C. M. Martin. 1975. Effects of diuretic states on collecting duct fluid flow resisance in the hamster kidney. *Am. J. Physiol.* 229:13–17.
14. Moore, L. C., J. Schnermann, and S. Yarimizu. 1979. Feedback mediation of SNGFR autoregulation in hydropenic and DOCA- and salt loaded rats. *Am. J. Physiol.* 237:F63–F74.
15. Navar, L. G. 1978. Renal autoregulation: perspectives from whole kidney and single nephron studies. *Am. J. Physiol.* 234:F357–F370.
16. Quinn, M. D., and D. J. Marsh. 1979. Peritubular capillary control of proximal tubule reabsorption in the rat. *Am. J. Physiol.* 236:F478–F487.
17. Sakai, T., E. Hallman, and D. J. Marsh. 1986. Frequency domain analysis of renal autoregulation in the rat. *Am. J. Physiol.* 250 *(Renal Fluid Electrolyte Physiol. 19)*:F364–F373.
18. Schnermann, J., A. E. G. Persson, and B. Agerup. 1973. Tubuloglomerular feedback: nonlinear relationship between glomerular hydrostatic pressure and loop of Henle perfusion rate. *J. Clin. Invest.* 52:862–869.
19. Shimada, S. G. and D. J. Marsh. 1979. Oscillations in mean arterial blood pressure in conscious dogs. *Circ. Res.* 44:692–700.
20. Von Rosenberg, D. U. Methods for the numerical solution of partial differential equations. Elsevier/North Holland, New York. 1969.
21. Welling, L. W., and D. J. Welling. 1978. Physical properties of isolated perfused basement membranes from rabbit loop of Henle. *Am. J. Physiol.* 234:F54–F58.
22. Wright, F. S. 1982. Flow-dependent transport processes: filtration, reabsorption, secretion. *Am. J. Physiol.* 243:F1–F11.
23. Young, D. K., and D. J. Marsh. 1981. Pulse wave propagation in rat renal tubules: implications for GFR autoregulation. *Am. J. Phys-iol.: Ren. Fluid Elec. Physiol.* 240:F446–F458.